POTENTIALS AND LIMITS OF SPACE OBJECT OBSERVATIONS AND DATA ANALYSES USING RADAR TECHNIQUES

D. Mehrholz

Research Establishment for Applied Science (FGAN),
Research Institute for High Frequency Physics (FHP),
D-5307 Wachtberg-Werthhoven, Germany.

ABSTRACT

Ground based radars are well suited to observe space objects due to their all-weather and day-and-night performance, however, the radar power budget will always be a limiting factor for detection of small objects at high ranges. The paper highlights potentials and limits of radar based methods to compute current orbital elements, to assess space object dimensions, shape, attitude and mass, to predict orbital lifetime and reentry windows, to compute range profiles and to reconstruct object images. Particular attention is given to the problem of improving the reliability of the mean motion n and its first derivative dn/dt the data of which are recorded in Two-Line-Elements (TLE). The accuracy of these data is essential for tracking, lifetime predictions, and mass assessments. An algorithm is suggested with which improved data can be computed from sets of TLE.

1. INTRODUCTION

The debris situation is of concern to the construction and operation of satellites in low Earth orbits (LEO) as well as in geostationary orbits (GO). The need for accurate risk assessments call for appropriate statistical and/or deterministic models of the current debris environment and its future development. Expected results achieved with such models are flux and collision rates, fragmentation laws after explosions or collisions, and precise orbital lifetime and decay rates. However, nonavailability and lack of data and a limited understanding of the generation of debris are responsible for severe uncertainties in these models. It is hoped that new measurements and improved modelling will reduce some uncertainties, but one has to keep in mind, that the prediction accuracy of future space activities of space faring nations has also a major influence on the validity of modelling results (Refs. 1 - 3).

The quality of environment models and the success of preventive measures (debris avoidance, collision avoidance, shielding, active debris removal) strongly depend on the precise knowledge not only of the number of debris per range bin but also of certain physical characteristics of the individual objects, like size, shape, mass, attitude, aerodynamical and material properties. Therefore radar, optical, and infrared measurements of a large number of orbital objects with known and unknown dimensions have been collected by many organisations from a variety of *Earth based sensors*. Most of these sensors are part of the U.S. Space Surveillance Network (SSN). Data from sensors outside the U.S. SSN are rare and usually not available. The employment of *space based sensors* is limited today to assessments of the orbital population of very small debris; results were achieved from examining windows of returned spacecraft or from experiments like LDEF (Long Duration Exposure Facility).

The only radar in Germany, capable to observe space objects, is the FGAN High Power Radar System. Since the reentry of KOSMOS-954 in January 1978, FGAN was regularly requested to advice the Federal Minister of Interior in all matters of decaying high risk space objects. FGAN's advice is based on their own radar measurements and analysis results. In some cases FGAN radar data and analysis results have been provided to external users (Refs. 4, 5).

2. FGAN HIGH POWER RADAR SYSTEM

At Wachtberg-Werthhoven, Germany, about 20 km south of Bonn, the German Defence Research Organisation FGAN (Forschungsgesellschaft für Angewandte Naturwissenschaften) operates a High Power Radar System. This system, being able to track and to image aircraft, satellites, and space debris, was developed to assist experimental radar research. It is composed of three main subsystems: a 34-m parabolic dish antenna, a L-band tracking radar, and a Ku-band imaging radar.

2.1 34-m Parabolic Dish Antenna

The core of the experimental radar system is a highly engineered and fully computer controlled elevation-over-azimuth pedestal mount. It supports a 34 m diameter parabolic dish antenna. The feed arrangement is based on the Cassegrain principle. The instrument is shielded from atmospheric influences by a rigid radome with 49 m diameter (Fig. 1).

2.2 L-Band Tracking Radar

The monopulse tracking radar operates at 1.333 GHz. High frequency impulses of typically 1 ms pulse length are generated and fed to a 4-horn monopulse feed via filters, wave guides, rotary joints and transmitted as circular polarized signals.

The signal processing concept is fully coherent and based on modern correlation techniques to support

target tracking in direction (elevation and azimuth) as well as in range and range rate. The corresponding control loops are computer controlled. Sufficient range resolution is achieved by pulse compression (binary phase shift keying).

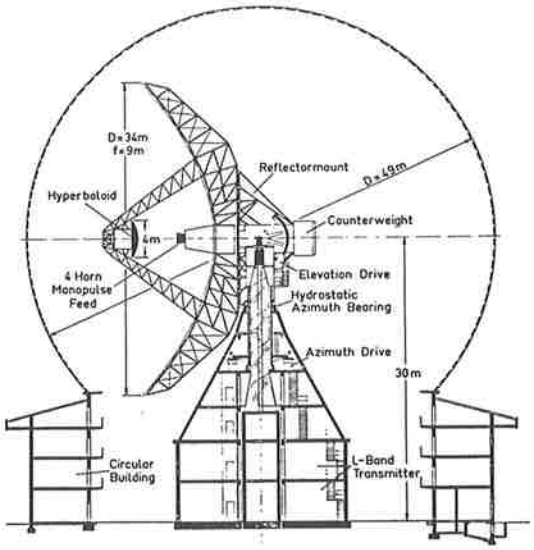

Figure 1. 34-m parabolic dish antenna at Wachtberg-Werthhoven.

The L-band data, measured with pulse repetition frequency (PRF), contain: target direction (azimuth and elevation), slant range, range rate, echo signal amplitude and phase. In addition time data (UTC, universal time coordinated), the transmitted peak power, and weather data (temperature, relative humidity, and air pressure) are recorded to cope with tropospheric refraction influences (Ref. 6).

2.3 Ku-Band Imaging Radar

The imaging radar operates at 16.7 GHz simultaneously with the tracking radar on the same target. The transmitter contains a wide band travelling wave tube (TWT) amplifier. At the time being only right hand circular polarized (RH) pulses are transmitted. The reception channel can be switched either to the RH or to the LH (left hand) port of the Ku-band feed system.

A chirp generator generates linear, frequency modulated impulses (LFM) of 800 MHz bandwidth having 256 μs pulse length (corresponding to 0.25 m range resolution, Hamming window). The received radar echo is de-ramped, down-converted and fed to a quadrature demodulator, gaining an in-phase signal (I) and a signal which is 90° phase-shifted (Q). The I,Q-components are filtered, digitized and stored as 1024 complex samples for each echo on computer disk for further processing together with transmitted peak power and time data (Ref. 6).

3. RADAR MEASUREMENTS AND ANALYSIS

3.1 Orbit Prediction and Determination

The orbital motion of a point mass about the Earth is governed primarily by the attraction between Earth and point mass (two-body case or KEPLERIAN orbits). Even for objects in geostationary orbits (altitude of 36.000 km), the gravitational effects of sun, moon and planets are very small. Unlike the multi-body problem, the two-body case can be solved analytically. In reality we are not dealing with point masses, but with space objects orbiting the Earth and there will be other forces acting upon the orbital motion. The actual trajectories of these objects are conceived as perturbed KEPLERIAN orbits. The most important perturbing forces are due to: asphericity of the Earth, aerodynamic effects, lunar and solar attraction, radiation pressure, and electromagnetic effects.

At FGAN prediction and determination of the orbital motion is based on the definition of mean orbital elements according to the theory of BROUWER and LYDDANE. The analytical solution of drag-free satellite motion allows fast realtime prediction of observation vectors (time, azimuth, elevation, range, and range rate) as well as fast determination of orbital elements (e.g. TLE) from radar data of only one satellite pass (Ref. 7). For a thorough orbit analysis a numerical integration of the equations of motion, including all relevant perturbations, is used. Of course, for this computation radar data of three to four consecutive passes are required.

Fig. 2 shows a L-band radar measurement protocol of MIR (object 16609, 86 17 A) from 12:51:47, 22 January 1992. The protocol contains a radar cross-section (RCS) plot, a polar plot to describe the observation scene, a range plot and a Doppler plot, a set of mean orbital elements computed from the tracking data, and data for the closest point of approach (CPA). These kind of protocols are used to determine LH or RH passes and to aid in visualisation of RCS behaviour, range, range rate, duration of observation, aspect angle, and mode of stabilisation.

The observation of space objects having orbits heavily perturbed by air drag using a "pencil-beam" radar calls for accurate mean motion data and acceptable assessments of the first and second derivative of the mean motion. All data are provided in sets of TLEs. Experience shows however, that in many cases the reliability of these data is insufficient. This holds especially for objects during reentry and for such cases where the mean motion n was badly assessed. Computation of the derivatives dn/dt and d^2n/dt^2 from the TLE history of mean motion data will generate unusable results. Therefore consider that the mean anomaly M gives the position of the satellite with respect to the perigee. Having two TLEs at different epoch t_i one could compute for $t=(t_1+t_2)/2$ an average mean motion $\bar{n}$:

$$\bar{n} = (M_2 - M_1 + 2k\pi)/(t_2 - t_1) = \Delta M/\Delta t.$$

The term $2k\pi$ takes care of k completed orbits in the time interval Δt. The problem is, that the perigee of a nearly circular orbit is not very well defined. This problem can be avoided by analysing $(M+\omega)$ instead of M, where ω represents the argument of the perigee:

$$\bar{n} = [(M_2+\omega_2+2k\pi) - (M_1+\omega_1) - (\omega_2-\omega_1)]/\Delta t \quad (1).$$

The quotient $(\omega_2-\omega_1)/\Delta t=\Delta\omega/\Delta t$ can be assessed using the well known relation between $d\omega/dt=\dot{\omega}$ and the mean motion, eccentricity, and inclination (Ref. 8). The factor k=1, 2, 3, ... follows from a plausible assumption for n. This algorithm provides even for unfavourable observations reliable mean motion data.

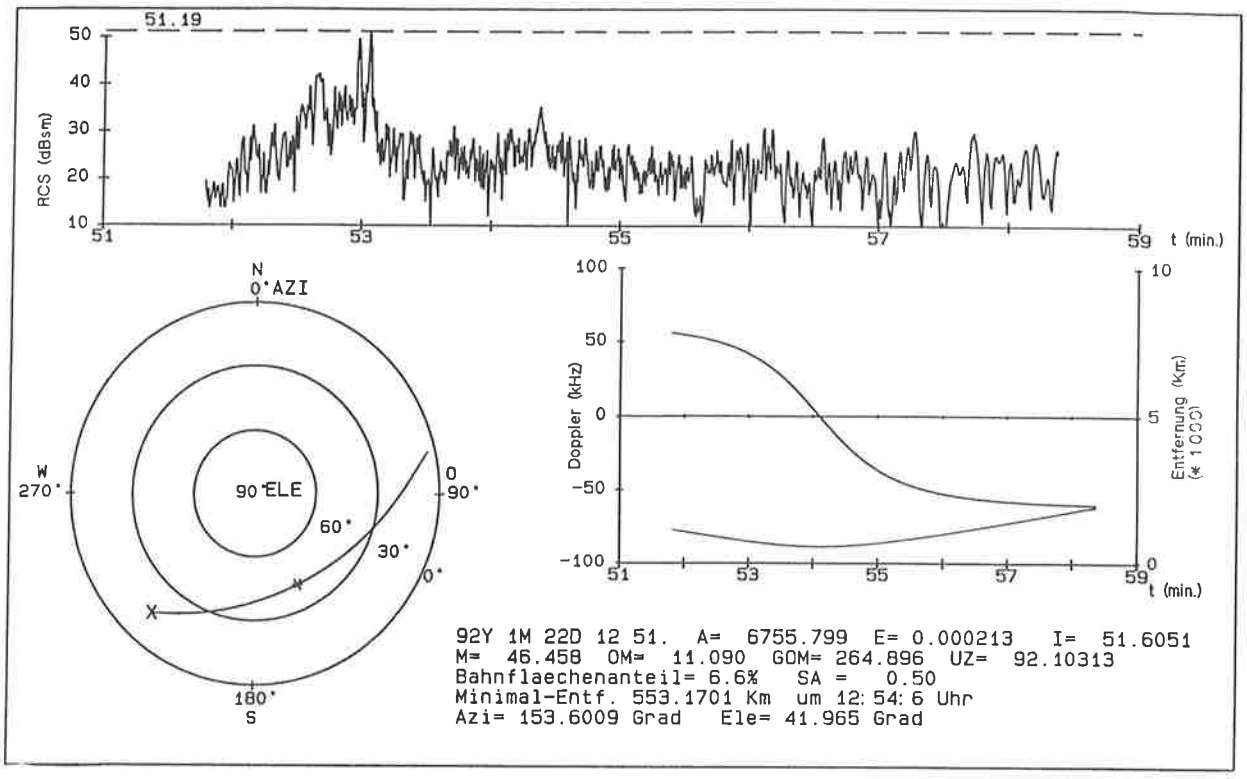

Figure 2. L-Band radar measurement protocol, MIR (object 16609, 86 17 A) measured 12:51:47, 22 January 1992. RCS data are uncalibrated, correction by subtraction of 2.1 dB in this case, ("x": start of measurement, "*": CPA).

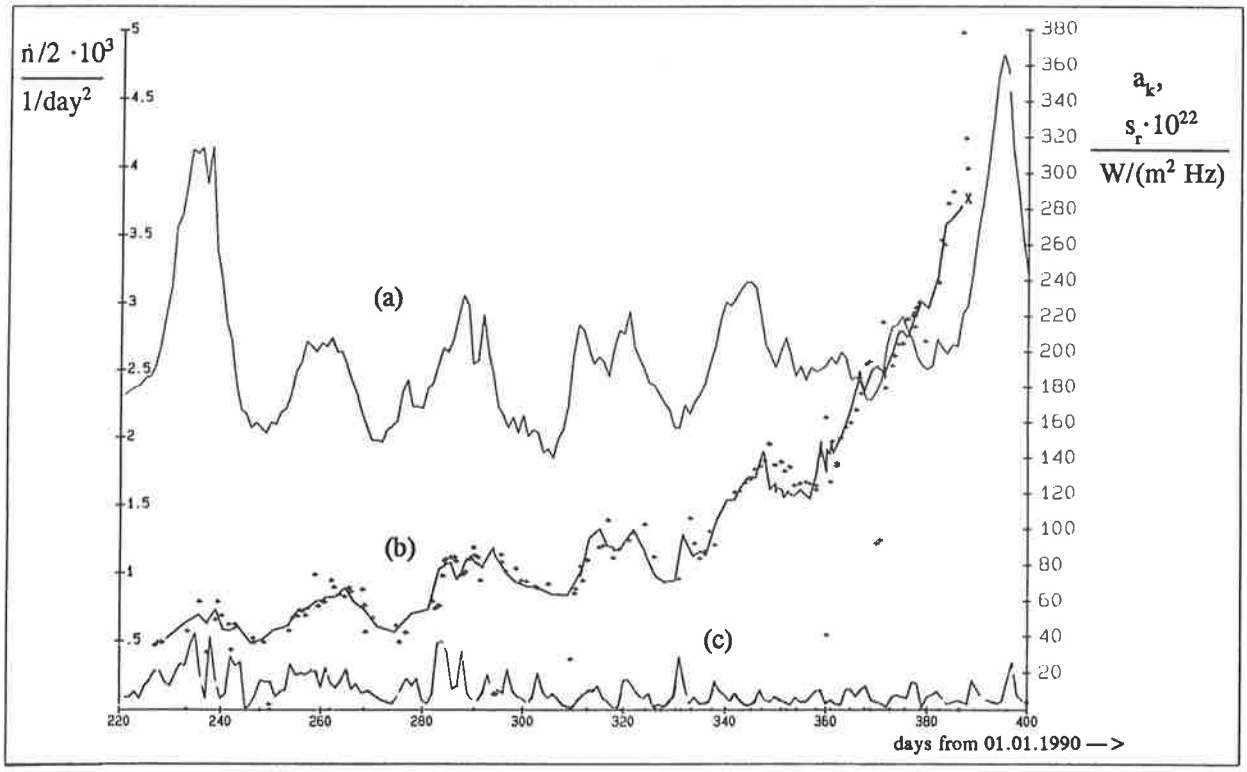

Figure 3. Development of the first derivative $\dot{n} = dn/dt$ of the mean motion n of SALYUT-7/KOSMOS-1686 (object 13138, 82 33 A) (plot b), solar radiation s_r (plot a), and geomagnetic activity a_k (plot c), $\Delta t = 1$ day.

From the history of $\bar{n}$ the derivatives dn/dt and d^2n/dt^2 can be computed. Acceptable results were achieved by selecting $\Delta t = 24$ hours, however, in the reentry phase (last three to four days) it is worthwhile to set Δt equal to the time for one orbit. Fig. 3 shows the situation for the decay of SALYUT-7/KOSMOS-1686.

The "+" in plot (b) mark data for the first derivative dn/dt as recorded in TLEs. Erroneous data are visible. The solid line of plot (b) was generated using the suggested algorithm (Eq. 1). The impact of the solar activity, represented by the 10.7 cm radiation, and the geomagnetic activity on dn/dt becomes clear.

3.2 Orbital Lifetime and Mass Assessments

The motion of space objects at less than 1000 km altitude (velocities of about 7.8 km/s) is apart from gravitational forces mainly affected by aerodynamic forces. The major part will be a drag force, acting opposite to the velocity vector. Lift and side forces will occur too, depending on the shape of the object. The atmospheric density varies with altitude and is a function of solar activity, disturbances of the geomagnetic field, and season.

3.2.1 Orbital Lifetime

Adopting an approximated, analytical solution of the LAGRANGE planetary equations for the mean motion n and orbit eccentricity e, it can be shown that the orbital lifetime L is inversely proportional to dn/dt (Refs. 9, 10):

$$L = \frac{3}{4} \cdot e \cdot \frac{n}{dn/dt}; \quad (0.03 \leq e \leq 0.2) \qquad (2)$$

Therefore, the accuracy of the predicted lifetime depends a lot on the estimation of n and dn/dt (Eq. 2). At FGAN the orbital lifetime of a space object is predicted with a computer assisted approach, based on King-Hele's analytical method (Refs. 9 - 11). The necessary information are taken from NASA or FGAN TLEs last of which are computed from FGAN radar data. The accuracy for short-term and medium-term predictions, based on this approach, is about $\pm$ 10% of the estimated lifetime. In general the accuracy is good enough to predict the correct reentry orbit. However, independent whether this analytical method or numerical integration is used to predict the reentry orbit, incidents like a geomagnetical storm or a sun burst will cause much worse accuracy. It is important to note that reliable results can be achieved only, if during the remaining lifetime there is: no change of object attitude, no change of object configuration, no manoeuvre, and no abnormal development of high-atmosphere density.

3.2.2 Mass Assessments

Estimation of the mass m of a space object is based on assessments of the ballistic coefficient B, of the drag coefficient c_D, and of object's average reference area A (Eq. 3):

$$B = c_D \cdot A/m \qquad (3)$$

$$\frac{da}{dt} = -\frac{2a}{3n} \cdot \frac{dn}{dt} = -\rho \cdot B \cdot (a \cdot G \cdot m_E)^{1/2} \qquad (4)$$

Eq. 4 describes for circular orbits the relation between the ballistic coefficient B and the derivative da/dt of the orbit radius a and the derivative dn/dt of the mean motion n. The first part of Eq. 4 results from differentiation of the 3rd KEPLERIAN law. The atmospheric density ρ is determined with a suitable air model (e.g. CIRA-88). The product of the gravitational constant G and the mass m_E of the Earth is a constant factor. The average reference area A depends on object size, shape, and attitude. The drag coefficient c_D can be assessed knowing size, shape, attitude, orbit altitude, and surface properties of the object (Ref. 12).

At FGAN these quantities are gained from analysis of narrow band and high resolution radar data (orbital elements, radar signatures, range profiles, and radar images). The accuracy of mass assessments is about 10-20% with the same assumptions as stated for lifetime predictions. The largest uncertainties are in the determination of atmospheric density ρ and the drag coefficient c_D.

3.3 Estimation of Size, Shape, and Attitude

There are several radar methods of varying efficiency (depending on the coherence of radar data and complexity of the target) applicable to assess size, shape, and attitude of a target (Refs. 13, 14). Radar data analysis of space objects, especially space debris is, apart from a few exceptions, a rather difficult task. Even if one is satisfied with a crude estimate, a lot of observations and sophisticated analyses are necessary. The following is a brief discussion of approaches, based on narrow band and high resolution radar data, which have been investigated at FGAN.

3.3.1 Noncoherent methods for narrow band radar data analysis

- Interpretation of radar signatures, e.g. indicators to specular returns, characterisation of the underlaying pattern of fast rotating objects and type of stabilisation, determination of rotation period and maximum RCS (Fig. 4).

- Statistical analysis of RCS measurements of space debris to gain mean and median RCS data (Ref. 15). Fig. 4 shows a L-band RCS plot (scaled in dBsm, which is decibel above one square meter). From inspection of the fluctuation in this plot it is evident, that the object is in a complex rotation. Assuming that an object can rotate about three orthogonal axes, the shortest rotation period visible in the plot is about 80 s. The second diagram in Fig. 4 presents the result of a statistical analysis of the RCS plot. Shown are cumulative mean, median, and standard deviation computed in the linear domain and scaled in square meter. The data describe the "radar size" of the object, in this case at L-band frequency (1.333 GHz). It depends on object's shape and size in terms of wavelength how far this "radar size" represents the true geometrical size of the object. This result was achieved with data from a time interval of 450 s of one satellite pass. Analysing data from 12 passes, with observation intervals between 400 and 800 s, the averaged mean RCS becomes 6.13 m^2 with 1.56 m^2 standard deviation (std), the averaged median RCS is 3.36 m^2 with 0.47 m^2 std. A possible reason for the relative large standard deviations might be the fact, that due to the complex, slow rotation not all aspect angles have been measured during one observation interval.

- Verification of shape and attitude by calculation of the RCS with physical optics or physical theory of diffraction techniques, using significant RCS features like specular returns.

- Reconstruction of the radius profile function of a metallic, convex body of revolution with geometrical optics from RCS data, which must be known for all aspect angles.

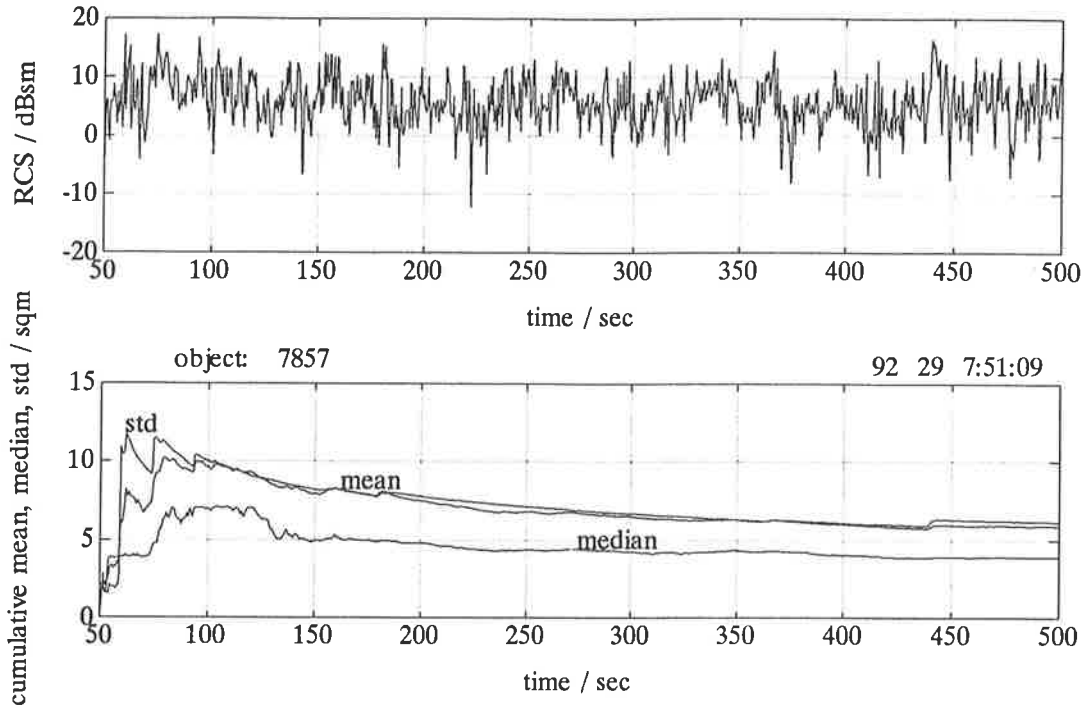

Figure 4. Top: Calibrated L-band RCS plot of object 7857 (debris from LANDSAT-1 launch), start 07:51:50, end 07:59:20 on 29 January 1992. Bottom: Cumulative mean, median, and standard deviation (std) of the L-band RCS computed in the linear domain and scaled in square meter.

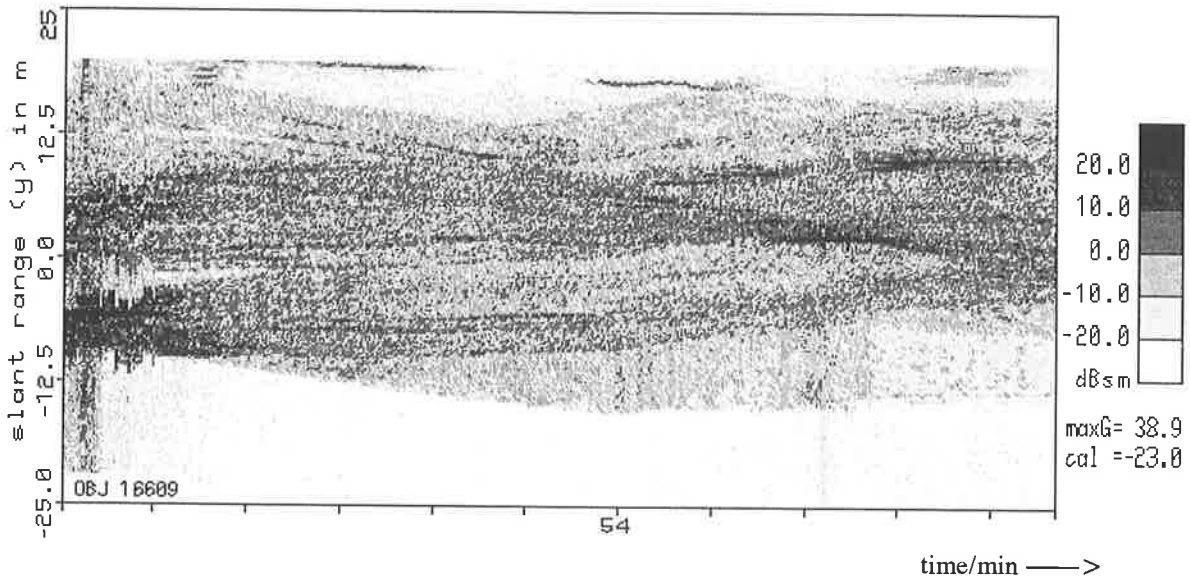

Figure 5. RTI plot of MIR (object 16609, 86 17 A), measured on 22 January 1992 (cf Fig. 2), 12:53:00.2 - 12:54:46.9, radar frequency 16.7 GHz (17.96 mm wavelength), bandwidth 800 MHz, range resolution 0.25 m, range profiles computed from 106.7 s observation interval around the CPA, radar is looking in y-axis direction.

- Fourier analysis of RCS data of a rotating object over a small aspect angle interval yields the cross-range projection of apparent distances between pairs of scatter centres.

3.3.2 Coherent methods for narrow band radar data analysis

- Reconstruction of the radius profile function of a metallic convex body of revolution from backscattered coherent field data of large aspect angle intervals by evaluation of the physical optics of diffraction integral.

- Fourier transform of backscattered coherent field data within a small integration interval yields the cross-range projection of scatter centres, 2-dimensional imaging is possible.

3.3.3 Coherent methods for high resolution radar data analysis

- Computation of range profiles, which are 1-dimensional scatter centre distributions, projected on radar line-of-sight (LOS), to estimate the object dimension in range direction and to assess the attitude. Fig. 5 shows a range-time intensity (RTI) plot

of the stabilised space station MIR, measured 22 January 1992, 12:53 (UTC), around CPA, PRF = 55.6 Hz, RCS_{max} = 38.9 dBsm. The development of the scatter centre situation due to aspect angle changes are clearly visible.

- Computation of radar images, which are presentations of the 2-dimensional scatter centre distributions, to gain information on size, shape, and attitude. A well established method to generate radar images is the *range-Doppler imaging* (RDI) approach, or equivalent in meaning: the *inverse synthetic aperture radar* (ISAR) approach.

  Resolution in slant range (y-direction, Fig. 6) is obtained by signal bandwidth. Resolution in cross-range (x-direction) is obtained by Doppler-frequency analysis, i.e. by generating a synthetic aperture for which a relative rotation (aspect angle change) between object and radar is required. It turns out that the resolutions in range and cross-range are in principle independent of range (of course, the signal-to-noise ratio must be sufficient and the necessary synthetic aperture angle must be attainable). This highly important fact as well as the day-and-night and all-weather capability of radar make RDI a valuable tool for long-range surveillance. Fig. 6 presents a radar image of the space station MIR, computed from data as shown in Fig. 5.

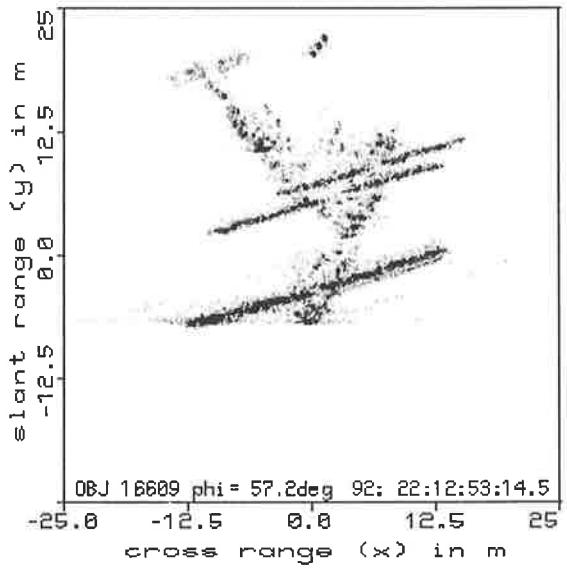

Figure 6. Radar image of MIR (object 16609, 86 17 A), computed from high resolution radar data, measured on 22 January 1992 (cf Fig. 5).
Radar frequency 16.7 GHz (17.96 mm wavelength), bandwidth 800 MHz, resolution 0.25 m.
Target range 665.52 km, range rate -4.00 km/s, elevation angle 32.61 deg.

4. ACKNOWLEDGEMENTS

The author is indebted to Dr. K. Magura and his Team for providing RTI plots and radar images; to Mr. Kübbeler who implemented and tested the suggested algorithm; to Dr. Leushacke for the statistical analysis of RCS measurements; and to the Radar Team of the author's division having designed and built the radars, and are performing regular measurements and analysis of radar data of selected space objects.

5. REFERENCES

1. Kessler, D.J., *Orbital debris environment for spacecraft in low Earth orbit*, Paper AIAA 90-1353, AIAA/NASA/DOD Orbital Debris Conference: Technical Issues & Future Directions, April 16-19, Baltimore, MD, 1990.

2. ESA SP-1109, *Space debris*, November 1988.

3. NASA/DOD, *Report on orbital debris*, February 1989.

4. Mehrholz, D., *Satellite observations with a single radar tracking station*, in ESA SP-246, Re-entry of Space Debris, Proc. of an ESA Workshop, 24-25 September 1985, 1986.

5. Mehrholz, D. and Magura, K., *Radar tracking and observation of 'noncooperative' space objects due to reentry of SALYUT-7/KOSMOS-1686*, in ESA SP-345, The Reentry of SALYUT-7/KOSMOS-1686, Proc. International Workshop, ESOC, Darmstadt, 9 April 1991, 1991.

6. Mehrholz, D., Magura, K., Rustemeier, M., Steinheuer, B. and Kübbeler, K.H., *Results of radar observations on RADCAT from 9 August 1989*, TR No. 1-90, FGAN-FHP, Wachtberg 1990.

7. Peters, H.G., *Methods for orbit predictions used at the FGAN-FHP*, in ESA SP-246, Re-entry of Space Debris, Proc. of an ESA Workshop, 24-25 September 1985, 1986.

8. Kozai, Y., *The motion of a close Earth satellite*, Astron. Journal 64, Page 367-377.

9. King-Hele, D.G., *The prediction of satellite lifetimes*, RAE, TR 87030, 1987.

10. King-Hele, D.G., *Method for predicting satellite orbital lifetimes*, RAE, TR 77111, 1977.

11. Peters, H.G., *Theoretical background of the prediction methods of satellite lifetimes used at FGAN-FHP*, SR No. 22-92, FGAN-FHP, Wachtberg 1992.

12 Johannsmeier, D., Koppenwallner, G., Mehrholz, D., Boettcher, R.D., *Determination of spacecraft parameters using radar data*, Hypersonic Technology Göttingen, ESA CR(P) 3327, 1991.

13. Bhattacharyya, A.K. and Sengupta, D.L., *Radar cross section analysis & control*, ISBN 0-89006-371-0, Artech House Inc., Norwood 1991.

14. Mensa, D.L., *High resolution radar cross-section imaging*, ISBN 0-89006-389-3, Artech House Inc., Norwood 1991.

15. Leushacke, L., Mehrholz, D., *Determination of physical characteristics of space debris*, Intermediate Reports No. 1 - 3, DARA Contract No. 50 ST 9003, FGAN-FHP, Wachtberg 1991/92.